Numerical investigation of non-Newtonian fluids in annular ducts with finite aspect ratio using lattice Boltzmann method

S. Khali, R. Nebbali, D. E. Ameziani, and K. Bouhadef

USTHB—Faculty of Mechanical and Process Engineering (FGMGP), Laboratory of Multiphase Transport and Porous Media (LTPMP), B. P. 32, El Alia Bab Ezzouar 16111, Algiers, Algeria

(Received 19 November 2012; published 3 May 2013)

In this work the instability of the Taylor-Couette flow for Newtonian and non-Newtonian fluids (dilatant and pseudoplastic fluids) is investigated for cases of finite aspect ratios. The study is conducted numerically using the lattice Boltzmann method (LBM). In many industrial applications, the apparatuses and installations drift away from the idealized case of an annulus of infinite length, and thus the end caps effect can no longer be ignored. The inner cylinder is rotating while the outer one and the end walls are maintained at rest. The lattice two-dimensional nine-velocity (D2Q9) Boltzmann model developed from the Bhatnagar-Gross-Krook approximation is used to obtain the flow field for fluids obeying the power-law model. The combined effects of the Reynolds number, the radius ratio, and the power-law index n on the flow characteristics are analyzed for an annular space of finite aspect ratio. Two flow modes are obtained: a primary Couette flow (CF) mode and a secondary Taylor vortex flow (TVF) mode. The flow structures so obtained are different from one mode to another. The critical Reynolds number Re_c for the passage from the primary to the secondary mode exhibits the lowest value for the pseudoplastic fluids and the highest value for the dilatant fluids. The findings are useful for studies of the swirling flow of non-Newtonians fluids in axisymmetric geometries using LBM. The flow changes from the CF to TVF and its structure switches from the two-cells to four-cells regime for both Newtonian and dilatant fluids. Contrariwise for pseudoplastic fluids, the flow exhibits 2-4-2 structure passing from two-cells to four cells and switches again to the two-cells configuration. Furthermore, the critical Reynolds number presents a monotonic increase with the power-law index n of the non-Newtonian fluid, and as the radius ratio grows, the transition flow regimes tend to appear for higher critical Reynolds numbers.

DOI: 10.1103/PhysRevE.87.053002 PACS number(s): 47.50.−d, 47.32.−y

I. INTRODUCTION

The fluid flowing between two concentric rotating cylinders of infinite length, known as Taylor-Couette flow, has been the subject of many experimental, analytical, and numerical studies. This is due to their industrial applications such as journal bearings, purification of wastewater, and oil drilling. It is well known that the stability of this kind of viscous flow was first considered experimentally and theoretically by Taylor [1]. Ever since their discovery by Taylor, the involved instabilities have been of perpetual interest for understanding the phenomenology associated to flow stability. However, in practice, the aspect ratio of the annular cavity is not large enough to apply the Taylor-Couette model. The ends effects become increasingly important as the aspect ratio is reduced: The circular Couette flow is not an exact solution for finite cylinders, and the tangential flow results always in main flow cellular cross, even for very small Reynolds numbers (Blennerhasset *et al*. [2] and Lücke *et al*. [3]). The solutions in the annulus of short cylinders may differ significantly from the ideal Taylor-Couette model, as was clearly demonstrated by Benjamin [4,5].

Benjamin [4] gave a qualitative description of the phenomenon of bifurcation and morphogenesis of the flow structure in the annular space with an aspect ratio of about 1. The experimental results were presented for the location of bifurcation critical points and flow profiles in the (Γ, η) plane.

Cole [6], using visualization and torque measurement in cylindrical ducts with free surfaces for an aspect ratio $H/d <$ 107 and a radius ratio $0.894 < \eta < 0.954$, showed that the value of the first critical Reynolds number changes little if the aspect ratio is not infinite, while the second critical Reynolds number is strongly affected when decreasing the aspect ratio.

Blennerhasset and Hall [2] analyzed theoretically the stability of a flow in a weak annulus gap for finite length cylinders. They showed that the problem allows multiple solutions, depending on the initial conditions. Mullin *et al*. [7] studied experimentally the transition from four to six cells in a short duct with a large annulus gap ($R = 0.507$) and discussed the hysteresis phenomenon according to the theory developed by Benjamin [4]. DiPrima and Eagles [8] have clarified the influence of the radius ratio on the stability of the Taylor flow. They showed that when Γ decreases, the number of unstable normal modes in a Couette system for a fixed Reynolds number decreases rapidly. They obtained a critical value of the radius ratio ($\eta = 0.65$) below which there is no cell instability.

The characteristics of flows in short cylinder cavities and dependency with respect to initial and boundary conditions have generated a growing interest. The works of Benjamin and Mullin [9], Cliffe [10], and Lücke *et al*. [3] were devoted to the bifurcation flow in a cylinder with an aspect ratio ranging between 0.4 and 6. They had two objectives: first, to describe the bifurcation diagrams and to locate bifurcation critical points in the (Γ, η) plane, and then explain how different modes can appear, either experimentally or numerically. These studies showed that (1) when the Reynolds number increases gradually, the cells in short cylinders are not directly due to the instability of the Couette flow, but to the growth of the cells generated close to the cavity extremities. (2) The coupling between the fixed end caps and the rotating inner cylinder has a strong nonlinear interaction that cannot be treated by the theory of perturbation.

The majority of studies on the Taylor-Couette flow focused on the Newtonian behavior. However, in numerous engineering applications such as oil well drilling, journal-bearing lubrication, food, cosmetics, and paints, the fluids often drift away from the Newtonian behavior. Thus, a growing number of authors take into account the rheological aspect by considering non-Newtonian fluids. Sinevic *et al*. [11] determined the onset of Taylor vortices by measuring the torque exerted by the fluid on the rotating inner cylinder for power-law fluids using carboxymethylcellulose (CMC) solution and Carbopol solutions. Measurements of the velocity fields for the Taylor-Couette flow were performed by Wereley and Lueptow [12] using particle image velocimetry. Lockett *et al*. [13] simulated the transition flow using the finite element method; the authors found that the stabilizing or destabilizing effect induced by the shear-thinning behavior depends on the radius ratio. Escudier *et al*. [14] investigated the flow structure in Taylor-Couette geometry with a radius ratio of 0.5. Axial and tangential velocity measurements were made using a laser Doppler anemometer.

During recent years, the lattice Boltzmann method (LBM) has received considerable attention from fluid dynamic researchers. It has been shown that it is an attractive alternative to classical numerical schemes due to its inherent advantages as simple implementation, high parallelizability, and great convenience of handling complicated geometries. Among studies concerning non-Newtonian fluids, handled with the LBM, Yoshino *et al*. [15] suggested a numerical scheme for incompressible non-Newtonian fluid flows based on the LBM. They applied this method to two test problems—the case of flows in reentrant corner geometry and the case of flows in a three-dimensional porous structure. Their simulations indicated that this method can be useful for practical non-Newtonian fluid flows. Wang and Bernsdorf [16] used the LBM in the analysis of a blood flow using the Carreau Yasuda model. A comparison has been made between non-Newtonian and Newtonian flows in a three-dimensional (3D) generic stenosis.

Studies on the axisymmetric variant of the LBM generally treat the flows of Newtonian fluids. Due to its capabilities to handle complex flow, the LBM has a great potential to simulate non-Newtonian fluid flows which are of high interest due to their wide applications in different industrial fields. These fluids exhibit a complex behavior different from that of Newtonian fluids, which adds to the complexity of the fluid flow problems. A typical geometry involved in these flows is the annular duct which is an axisymmetric configuration. Halliday and Hammond [17] first proposed an axisymmetric D2Q9 model and it seems very successful for simulating steady flow in straight tubes. The main idea of the model is inserting several spatial and velocity-dependent "source" terms into the two-dimensional (2D) lattice Boltzmann equation (LBE). However, Lee *et al*. [18] noticed that some terms relative to the radial velocity were missing in the axisymmetric D2Q9 model of [17]. These authors developed a more accurate axisymmetric LBM scheme.

Later, several authors developed their own scheme to simulate the axisymmetric flows using the LBM. Niu *et al*. [19] presented an extension of the idea of Halliday and Hammond [17] including the effect of the azimuthal rotation. The terms related to the rotation are considered as inertia forces. They used Taylor-series expansion and a least-squares-based lattice Boltzmann method for the transformed LBE and a second order explicit finite difference method for the azimuthal moment equation. To show the performance of the model, they also simulated the same problem by using the (3D) LBM. Peng *et al*. [20] extended Halliday's idea to the axisymmetric thermal systems. Besides the radial and axial velocity components solved by the lattice Boltzmann formulation, the azimuthal velocity component and the temperature are obtained using a finite differences scheme. Afterwards, Huang *et al*. [21–25] proposed a revised version of the D2Q9 model proposed by He and Luo [26] to improve the numerical stability and to reduce the compressibility effect. They developed a hybrid lattice Boltzmann scheme for axisymmetric flows with the rotation of the inner cylinder. The axial and the radial velocities were solved through inserting source terms into the two-dimensional lattice Boltzmann equation, while the azimuthal velocity and the temperature equations were discretized with a finite difference scheme. The used scheme was first validated by simulations of Taylor-Couette flows between two concentric cylinders; then the benchmark problem of melting flow in Czochralski crystal growth was simulated and correct results were obtained. Lee *et al*. [27] presented an accurate axisymmetric lattice Boltzmann D2Q9 model to simulate steady and pulsated flows in circular pipes. They introduced some improvement on the original model of Halliday and Hammond [17]. Zhou [28] proposed another axisymmetric scheme, suitable for general axisymmetric flows, where the force and source or sink terms were incorporated into the lattice Boltzmann (LB) equation naturally. In 2011, the same author presented a revised axisymmetric lattice Boltzmann method [29]. In 2012, Hongyan *et al*. [30] obtained an analytical solution of an axisymmetric lattice Boltzmann model for cylindrical Couette flows for non-Newtonian fluid.

The present work investigates the instability of the Taylor-Couette flow for Newtonian and non-Newtonian fluids, and the use of LBM in the cases of finite aspect ratios, where in many industrial applications the apparatuses and installation have finite dimensions with partly large boundary influence on fluid flow. The inner cylinder rotates while the outer one and the end walls are maintained at rest. The model proposed by Huang *et al*. [21] is adopted. The study is conducted for the case of an annular duct having an aspect ratio $\Gamma = 3.8$ which represents the finite column case with different values of Reynolds number and radius ratio. The velocity and stream function distribution along the annular duct were compared with analytical and numerical solutions. The friction factor was compared with the available experimental data. The combined effects of the Reynolds number, the radius ratio, and the power-law index on the flow characteristics were analyzed for an annular space of the finite column case.

II. LATTICE BOLTZMANN NUMERICAL METHOD

As has been previously mentioned, the standard LBM was developed for Cartesian coordinates systems. To handle axisymmetric problems with this method, without using a 3D lattice system, a source term is introduced in the original LB equation as was done by [21].

The three-dimensional axisymmetric Navier-Stokes equations are written in a pseudo-Cartesian form making the

following replacement:

$$(r,z)\rightarrow(x,y) \text{ and } (u_r,u_z,u_\theta)\rightarrow(u,v,w),$$
$$\partial_j u_j = \frac{-u_r}{r}, \tag{1}$$
$$\rho[\partial_t u_i+\partial_j(u_i u_j)] = -\partial_i P+\mu\partial_j^2 u_i+\frac{\mu u_i u_r}{r}-\frac{\mu u_i}{r^2}\delta_{ir}. \tag{2}$$

Bearing in mind that, in the standard LB equation, the recovered macroscopic momentum equation is written as

$$\rho[\partial_t u_i+\partial_j(u_i u_j)] = -\partial_i P+\partial_j[\mu(\partial_i u_j+\partial_j u_i)]. \tag{3}$$

Therefore we need to rewrite Eq. (2) as

$$\rho[\partial_t u_i+\partial_j(u_i u_j)] = -\partial_i P+\partial_j[\mu(\partial_i u_j+\partial_j u_i)]+\frac{\mu}{r}(\partial_r u_i+\partial_i u_r) - \frac{\rho u_i u_r}{r}-2\frac{\mu u_i}{r^2}\delta_{ir}. \tag{4}$$

Compared with the form in the (x, y) plane, the two terms in right-hand side of the above equation can be considered as body forces. Now we follow the idea of [17] and derive an LBE which recovers Eqs. (1) and (2) from an incompressible D2Q9 model. The discrete velocities of this model are as follows:

$$e_i=\begin{cases}(0,0) & i=0\\ \left(\cos\left[\frac{(i-1)\pi}{2}\right],\sin\left[\frac{(i-1)\pi}{2}\right]\right)c & i=1,2,3,4\\ \sqrt{2}\left(\cos\left[\frac{(i-5)\pi}{2}+\frac{\pi}{4}\right],\sin\left[\frac{(i-5)\pi}{2}+\frac{\pi}{4}\right]\right)c & i=5,6,7,8\end{cases}, \tag{5}$$

where $c=\delta x/\delta t$, and in our studies $c=1$.

Note that δx and δt are, respectively, the lattice spacing and time step. They are set to unity. The two-dimensional LBE describing 2D flow in (x, r) pseudo-Cartesian coordinates is constructed as follows:

$$f_i(x+ce_{iz}\delta_t,r+ce_{ir}\delta_t,t+\delta_t)-f_i(x,r,t) = \frac{1}{\tau}\left[f_i^{\rm eq}(x,r,t)-f_i(x,r,t)\right]+S_i(x,r,t), \tag{6}$$

where τ is the relaxation time, f_i is the density distribution function along the i direction, $e_i(e_{ix},e_{iy})$ is the particle velocity in the i direction, and $f_i^{\rm eq}$ is the corresponding equilibrium state distribution function, which can be written as

$$f_i^{\rm eq}(x,r,t)=\omega_i\frac{p}{c_s^2}+\omega_i\rho\left[\frac{e_i u}{c_s^2}+\frac{(e_i u)^2}{2c_s^4}-\frac{u^2}{2c_s^2}\right] \quad i=0,1,2,\ldots,8, \tag{7}$$

where $c_s=c/\sqrt{3}$ is the sound speed, p is the pressure and ρ is the fluid density. The constant factors ω_i differ from one model to another (in the D2Q9 they are given as $\omega_0=4/9$, $\omega_i=1/9$ for $i=1, 2, 3, 4$) and $\omega_i=1/36$ for i = 5, 6, 7, 8).

The constant relaxation time τ and the fluid viscosity ν are linked as follows:

$$\nu=(2\tau-1)\delta_x/6. \tag{8}$$

As the relaxation time approaches 0.5 kinematic viscosity goes to zero ($\nu\approx 0$), which makes the LBM instable. Thus, to avoid having no physical viscosity, τ must be greater than 0.5.

$S_i\ (z,\ r,\ t)$ is defined as a function of the space and the velocity. It can be expressed as

$$S_i=\delta_t S_i^{(1)}+\delta_t^2 S_i^{(2)}, \tag{9}$$

where $S_i^{(1)}$ and $S_i^{(2)}$ represent respectively, zero order and first order gradients of the macroscopic variables ρ, u. By performing a Chapman-Enskog expansion, the following developments are obtained (see, for instance, Huang *et al.* [21]):

$$S_i^{(1)}=-\frac{\omega_i\rho u_r}{r}, \tag{10}$$

$$S_i^{(2)}=\frac{\omega_i}{2r}\left[\partial_r\left(\frac{p}{\rho}\right)+\partial_z u_z u_r+\partial_r u_r u_r\right] +\frac{3\omega_i\upsilon}{r}\left(\partial_r u_z e_{iz}+\partial_r u_r e_{ir}-\frac{u_r e_{ir}}{r}\right) -3\omega_i\frac{u_r}{r}(u_z e_{iz}+u_r e_{ir})-\omega_i(1-\tau) \times\left(\frac{\partial_z u_r}{r}e_{iz}-\frac{u_r}{r^2}e_{ir}+\frac{\partial_r u_r}{r}e_{ir}\right)+3\omega_i\left(\frac{u_\theta^2}{r}e_{ir}\right). \tag{11}$$

For the velocity derivations in Eq. (11), the terms $\partial_r u_z, \partial_z u_r$, $\partial_z u_z$ and $\partial_r u_r$ all can be obtained through Eq. (12) with replacing $\alpha=z$, $\beta=r$; $\alpha=\beta=z$ and $\alpha=\beta=r$, respectively:

$$(\partial_\beta u_\alpha+\partial_\alpha u_\beta)=-\frac{1}{\rho\nu}\left(1-\frac{1}{2\tau}\right)\sum_{i=0}^{8}f_i^{ne}e_{i\alpha}e_{i\beta}+O(\varepsilon^2). \tag{12}$$

Only $\partial_z u_r$ is obtained by using a second order finite difference scheme; it is given by

$$(\partial_z u_r)_{i,j}=[(u_r)_{i,j+1}-(u_r)_{i,j-1}]/(2\delta_x). \tag{13}$$

In the streaming step, the new distribution function value obtained from Eq. (6) would propagate to the adjacent eight lattices. That procedure can be represented as follows:

$$f_i(z+ce_{iz}\delta_t,r+ce_{ir}\delta_t,t+\delta_t)=f_{i\_\rm new}(z,r,t). \tag{14}$$

The basic hydrodynamic quantities, such as the density ρ and the velocity components, are obtained through moment summations in the velocity space:

$$\rho(x,t)=\sum_i f_i(x,t),\ \rho u(x,t)=\sum_i e_i f_i(x,t). \tag{15}$$

III. PHYSICAL PROBLEM

We consider two coaxial cylinders with a finite length H. The inner cylinder of radius r_i rotates at an angular speed Ω while the outer cylinder of radius r_e and the end caps are kept at rest. The modified Reynolds number for the non-Newtonian fluids, based on the azimuthal velocity and the gap of the annulus, is defined as $\mathrm{Re}=\frac{(\Omega r_i)d}{\nu}$, where $d=(r_e-r_i)$ is the gap of the annulus and ν is the kinematic fluid viscosity.

Initially, a constant azimuthal velocity is imposed on the inner cylinder and the flow field is set to be stationary with a constant density ρ. $\eta=r_i/r_e$ is the radius ratio. In the present study, the aspect ratio $\Gamma=H/(r_i-r_e)$ was set to [1, 2, 3.8, 5,

8, and 10] for the finite case and 14.3 for the infinite column case, where H is the length of the annulus.

In order to formulate the problem, it is assumed that the flow in the annular gap is incompressible, laminar, and axisymmetric. It is known that in the commonly used power-law model, for non-Newtonian fluids, the viscosity varies with the local shear rate $\dot{\gamma}$ in the form

$$\mu = \mu_a \, |\dot{\gamma}|^{(n-1)}, \tag{16}$$

where n is the power-law exponent and μ_a is the apparent viscosity.

Note the case where $n = 1$ corresponds to the Newtonian fluid, in which μ_a corresponds to the viscosity of the Newtonian fluid. For a fluid with $n > 1$, the effective viscosity increases with shear rate, and the fluid is called "shear-thickening" or "dilatant fluid." In the case of a fluid with $0 < n < 1$, the effective viscosity decreases with shear rate, and the fluid is called "shear-thinning" or "pseudoplastic" fluid.

Regarding the relatively low rotation speed considered in the present study the constitutive relationship of the shear rate $\dot{\gamma}$ is given by

$$\dot{\gamma} = 2\left[\left(\frac{\partial u_r}{\partial r}\right)^2 + \left(\frac{u_r}{r}\right)^2 + \left(\frac{\partial u_z}{\partial z}\right)^2\right] + \left[r\frac{\partial}{\partial r}\left(\frac{u_\theta}{r}\right)\right]^2 + \left(\frac{\partial u_\theta}{\partial z}\right)^2 + \left(\frac{\partial u_r}{\partial z} + \frac{\partial u_z}{\partial r}\right)^2. \tag{17}$$

Coupling Eqs. (8) and (16), we obtain a shear-dependent relaxation time at each node in the lattice Boltzmann evolution.

The azimuthal velocity is obtained through the following equation by using first-order forward difference scheme in time and a second-order central difference scheme in space (Peng *et al.* [20]):

$$u_\theta^{n+1} = u_\theta^n + \delta_t\left[-\left(u_z^n\frac{\partial u_\theta^n}{\partial z} + u_r^n\frac{\partial u_\theta^n}{\partial r}\right) + \nu\left(\frac{\partial^2 u_\theta^n}{\partial z^2} + \frac{\partial^2 u_\theta^n}{\partial r^2}\right) + \frac{\nu}{r}\left(\frac{\partial u_\theta^n}{\partial r} - \frac{u_\theta^n}{r}\right) - \frac{u_r^n u_\theta^n}{r}\right]. \tag{18}$$

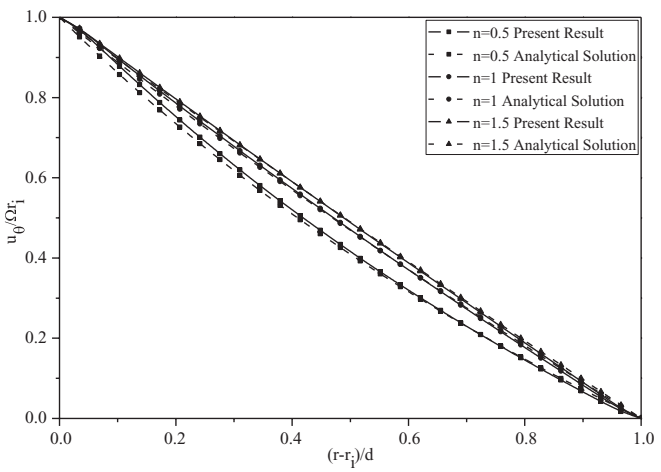

FIG. 1. Comparison of the azimuthal velocity with analytical solution for $\eta = 0.5$, $\Gamma = 3.8$, and $n = 1$.

TABLE I. Comparison of C_f versus Re values against results of Cognet [32].

Re	C_f Present results	C_f Cognet[a]	$(\varepsilon\%)_{\max}$
160.96	3.071	3.015	1.85
175.51	3.254	3.236	0.55
206.18	3.733	3.757	0.63
249.19	4.339	4.504	3.66
294.41	4.860	5.00	2.80

[a]Reference [32].

The local shear stress at the inner and outer wall is defined as

$$\tau = -\rho\nu\left[r\frac{\partial}{\partial r}\left(\frac{u_\theta}{r}\right)\right]_{r=r_i,r_e}. \tag{19}$$

The averaged shear stress over the annulus height and the averaged dimensionless friction factor are defined as

$$\tau_m = \frac{1}{H}\int_0^H \tau dz, \tag{20}$$

$$C_f = \frac{2\tau_m}{\rho\,(\Omega r_i)^2}. \tag{21}$$

IV. BOUNDARY CONDITIONS

Modeling of the boundary conditions is very important in numerical methods because they affect the overall accuracy and the stability of the numerical scheme. Two kinds of boundary conditions are used to describe the nonslip condition in the present work. On the inner cylinder the specular reflection is adopted while on the outer cylinder and the two end plates, the bounceback condition is used. These types of conditions suppose that the postcollision distribution function at the solid nodes with a velocity $-e_i$ is set equal to the postcollision distribution function at the fluid nodes with a velocity e_i.

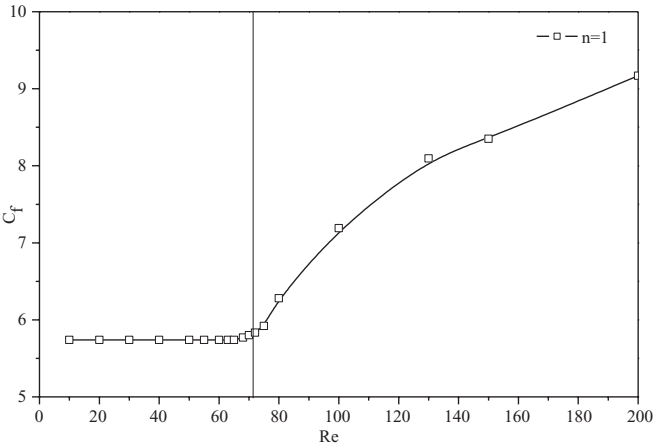

FIG. 2. Evolution of the friction factor against the Reynolds number for $\Gamma = 14.3$ and $\eta = 0.5$.

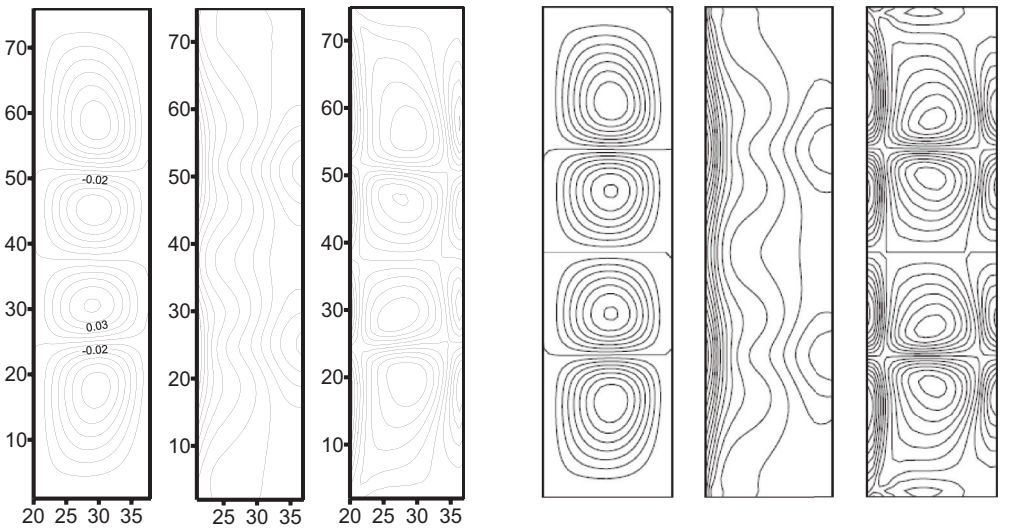

(a) Present work (b) Huang [21]

FIG. 3. Comparison of streamlines (left), pressure (middle), and azimuthal vorticity (right) fields against results of Huang *et al.* [21] for $n = 1$, Re $= 150$, $\eta = 0.5$, $\Gamma = 3.8$.

V. NUMERICAL RESULTS AND DISCUSSION

To verify the accuracy of the developed LBM code predicting the Taylor-Couette flow of non-Newtonian fluids, some validation tests were performed. Thus, the Newtonian cases are considered with two values of the aspect ratio equal to 3.8 and 14.3 which represent the finite column and the infinite column cases. For basic Couette flow, the present axisymmetric LBM code successfully recovers the analytical profile, given by the relation (22) for the infinite case (see, for instance, Brahim *et al.* [31]) of the Newtonian ($n = 1$), dilatant ($n = 1.5$), and pseudoplastic ($n = 0.5$) azimuthal velocity as is shown in Fig. 1.

$$u_\theta(r) = \frac{r}{r_i}\left[1 - \left(\frac{1}{r_e^{2/n}} - \frac{1}{r_i^{2/n}}\right)^{-1}\left(\frac{1}{r^{2/n}} - \frac{1}{r_i^{2/n}}\right)\right], \tag{22}$$

where r_i and r_e are, respectively, the dimensionless radii of the inner and the outer cylinder.

The computed values of the friction factor at the inner cylinder at the midheight of the annulus for a radius ratio $\eta = 0.909$ were compared with the measurements made by Cognet [32]. The results reported in Table I show that the maximum error is less than 3.67%.

Moreover, for the infinite Taylor column with an aspect ratio of $\Gamma = 14.3$ of a large radius aspect ratio ($\eta = 0.5$) filled with a Newtonian fluid, Fig. 2 shows the variation of C_f as a function of Reynolds number for the infinite annulus. The results show that the critical Reynolds number induced by the rotation of the inner cylinder is in good agreement with the critical value predicted theoretically (Re $= 68.2$; see for instance, Peng *et al.* [33]); the critical values were numerically determined through gradual increase in Re. One can note for Re approximately less than 68 the constancy of the friction factor indicating that the flow is in a stable regime, but for Re values above 68 the

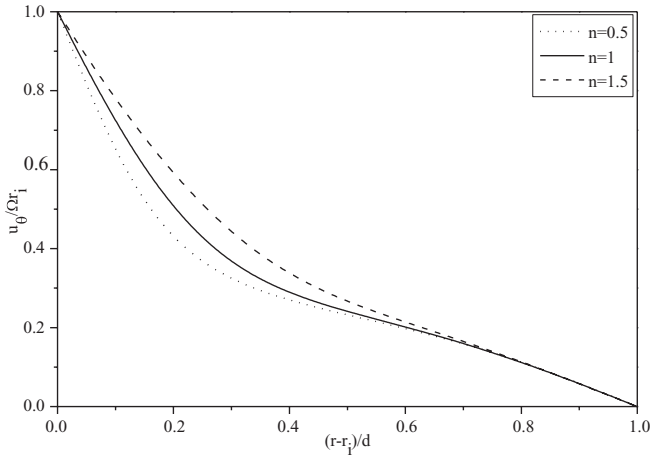

FIG. 4. Variations of the azimuthal velocity profiles for different fluids types for $\eta = 0.5$ and $\Gamma = 3.8$.

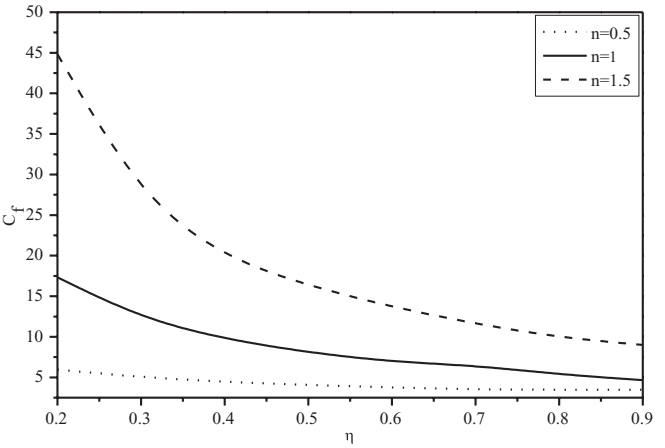

FIG. 5. Evolution of the friction factor versus the radius ratio η for different n, Re $= 100$, $\eta = 0.5$, and $\Gamma = 3.8$).

TABLE II. Comparison of Ψ_{max} for different Re values against literature results.

Re	Present work	Huang *et al.*[a]	Niu *et al.*[b]	Liu[c]	ε_{max}
85	4.903×10^{-2}	4.810×10^{-2}	4.859×10^{-2}	4.854×10^{-2}	1.82%
100	5.553×10^{-2}	5.501×10^{-2}	5.580×10^{-2}	5.542×10^{-2}	0.93%
150	6.361×10^{-2}	6.427×10^{-2}	6.387×10^{-2}	6.442×10^{-2}	1.25%

[a]Reference [21].
[b]Reference [19].
[c]Reference [34].

coefficient of friction increases significantly which indicates an unstable regime.

Finally, for an aspect ratio of 3.8 and the Newtonian fluid ($n = 1$), the efficiency of the developed LBM code was checked against results of Huang *et al.* [21], Niu *et al.* [19], and Liu [34]. The case of Taylor-Couette flow for Re = 85, 100, and 150 using mesh grids 20×76 was successfully simulated. Indeed, Fig. 3 shows that the isocontours of streamlines, pressure, and vortices present a good agreement with Huang *et al.* [21] results while Table II shows that the maximum deviation of Ψ_{max} does not exceed 1.82%.

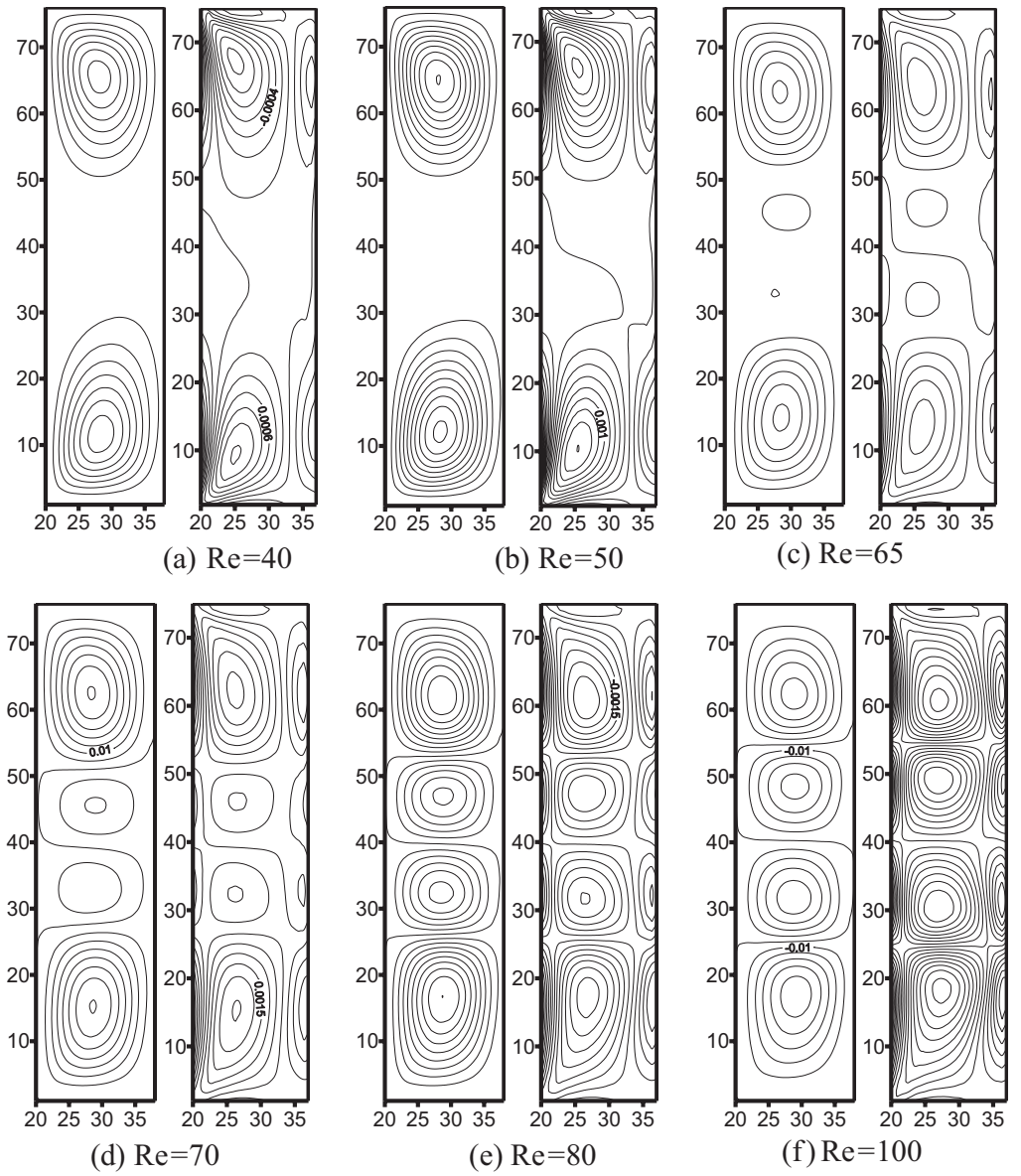

FIG. 6. Contours of streamlines (left) and vorticity (right) fields for $n = 1$, $\Gamma = 3.8$, and $\eta = 0.5$. (a) Re = 40, (b) Re = 60, (c) Re = 65, (d) Re = 68.4, (e) Re = 85, and (f) Re = 100.

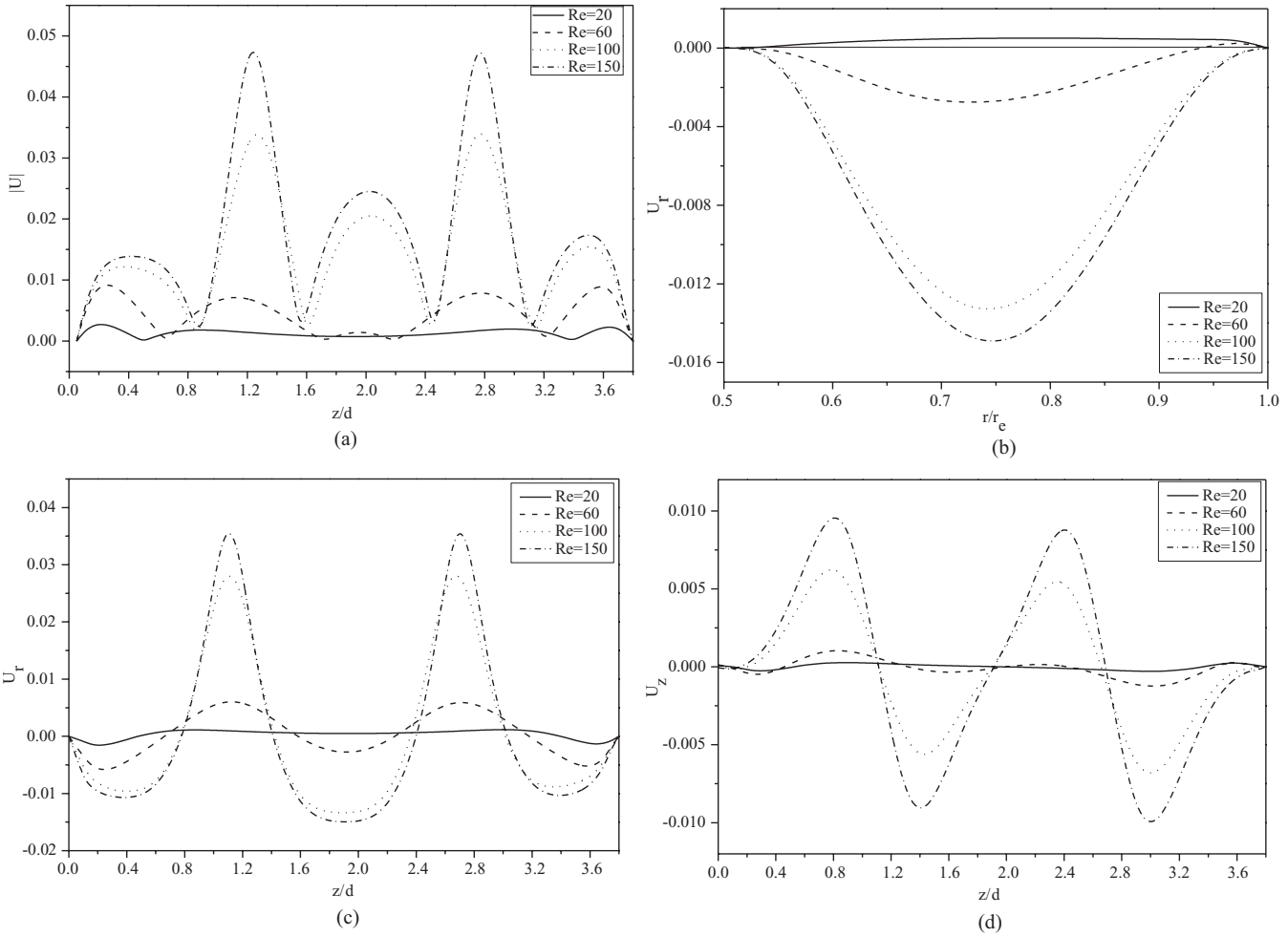

FIG. 7. Velocity profiles variations for $n = 1$ and different Re. (a) The modulus velocity along the vertical direction at $r = d/2$, (b) radial velocity along the radial direction at $z/d = 1.9$, (c) axial velocity along the radial direction at $r = d/2$, and (d) radial velocity along the axial direction at $r = d/2$.

Due to the numerous parameters controlling the flow configuration, all calculations are performed by setting the aspect ratio value of 3.8. The initial azimuthal velocity of the inner cylinder is set to 0.15, the mesh size to 20×76, and the radius ratio to 0.5. For the non-Newtonian fluid flows the exponent n was chosen in the range between 0.5 and 1.5 while the Reynolds number was varied from 20 to 150 [35–48].

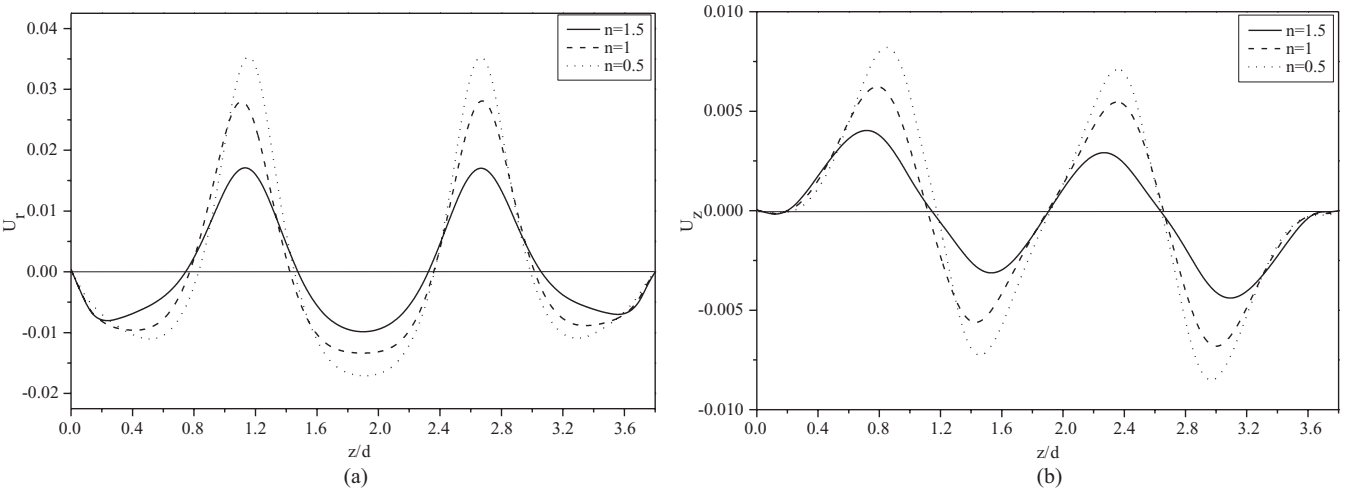

FIG. 8. Velocity profiles for different values of n and $\mathrm{Re} = 100$. (a) Radial velocity along z/d, and (b) axial velocity along z/d.

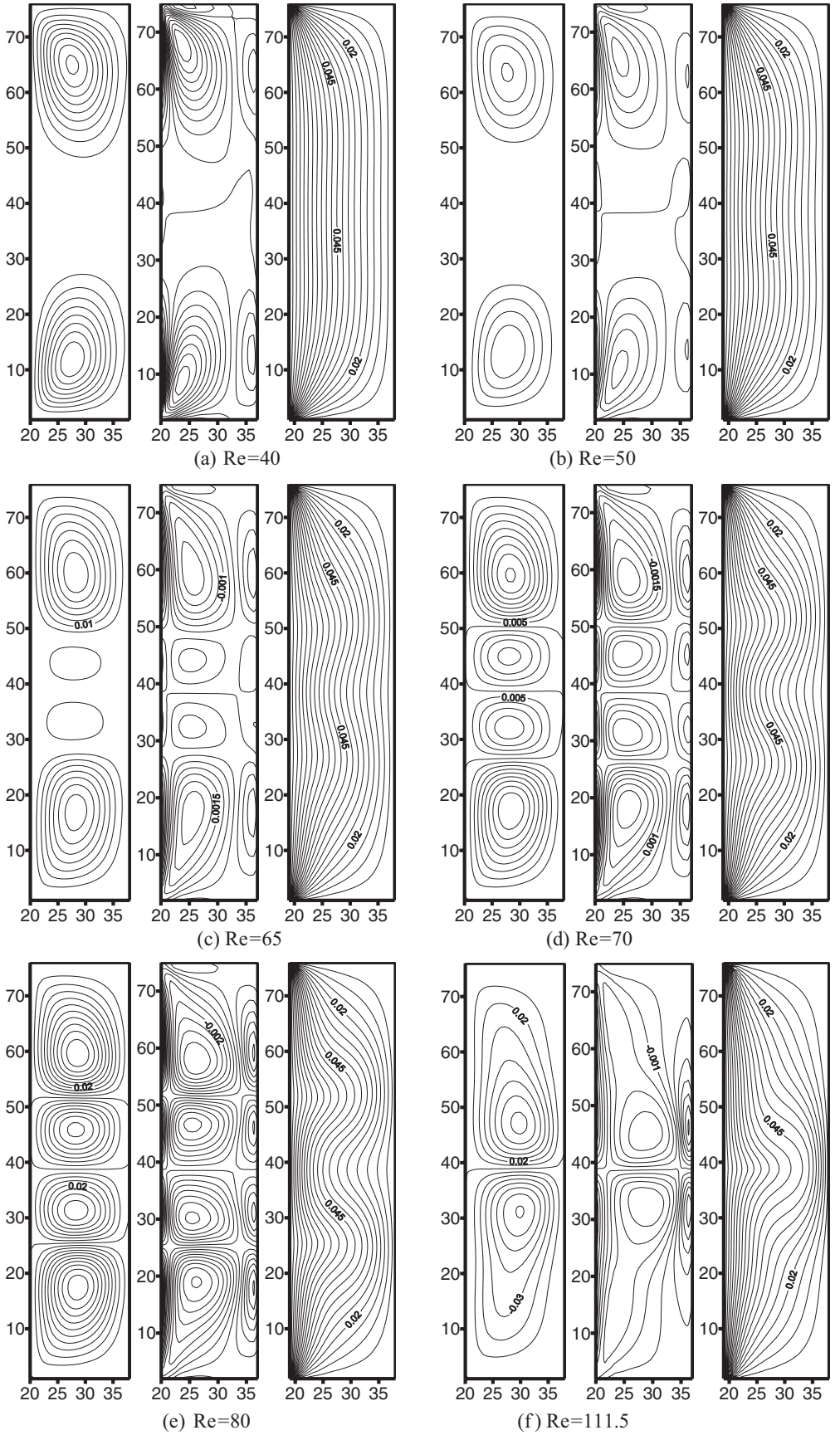

FIG. 9. Flow patterns streamlines (left), azimuthal vorticity (middle), and azimuthal velocity (right) for the pseudoplastic fluids ($n = 0.5$).

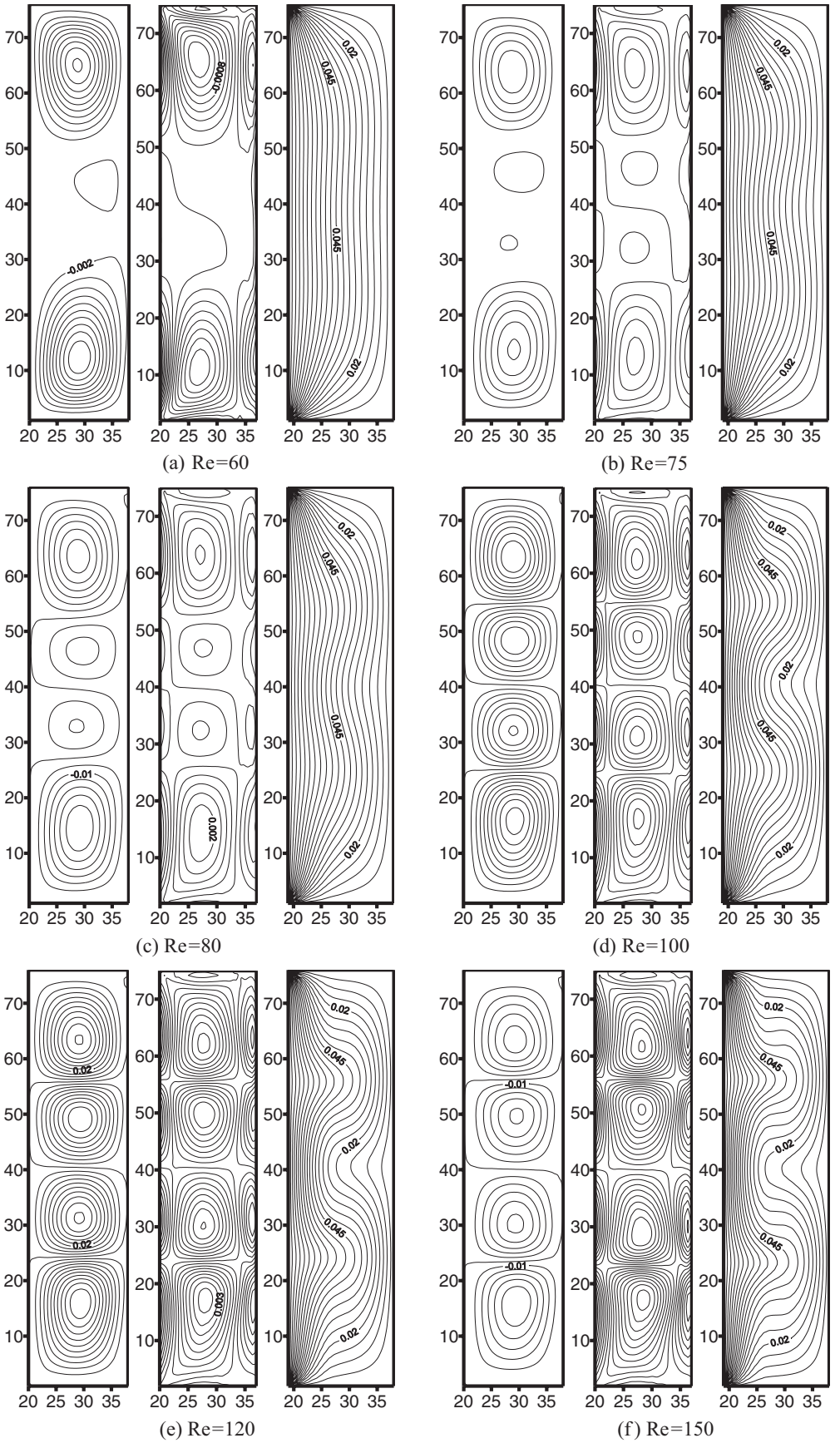

FIG. 10. Flow patterns streamlines (left), azimuthal vorticity (middle), and azimuthal velocity (right) for the dilatant fluids ($n = 1.5$).

Figure 4 illustrates the dimensionless azimuthal velocity along the radial position for different values of the power-law index n. It is shown that the velocity profile decays gradually along the radial position for the considered fluids. We note that the azimuthal velocity exhibits two distinct behaviors as a function of n in the space annulus. For approximately $0 < r < 0.7$, the augmentation of n increases the velocity modulus. When $r > 0.7$, the power-law index no longer has any effect on the velocity profile. Moreover, the azimuthal velocity gradients are more important for the pseudoplastic fluids than for the dilatant fluids.

Figure 5 shows the evolution of the friction factor, C_f, versus the radius ratio η for different values of n for $\mathrm{Re} = 100$. One can note that η influences strongly the friction factor of dilatant fluids ($1 < n < 1.5$) particularly for its low values. For pseudoplastic fluids ($0 < n < 1$), such impact is low, leading thus to practically a constant friction factor when η decreases. As n increases, the friction factor grows especially for small values of the radius ratio. This behavior can be explained by the fact that the apparent viscosity increases with n resulting in the increase of the friction coefficient.

The flow pattern is illustrated as contours of streamlines and vortices for the Newtonian fluid ($n = 1$) in Fig. 6 highlighting the effect of the Reynolds number. For $\mathrm{Re} = 40$, the flow structure is characterized by the so-called Ekman vortices on the end walls due to the nonslip condition. As Re increases, a second pair of cells begins to form in the central region of the annuli [Fig. 6(c)]. For further increase in Reynolds number, we note the onset of a weak pair of cells in the center of the annuli. The topological structure of the flow switches completely to the four-cell regime for a critical Reynolds number $\mathrm{Re}_c = 68.4$. Note that for $\mathrm{Re} > \mathrm{Re}_c$, the centrifugal force effect in the annulus prevails on the viscous forces and the flow is dominated by the laminar unstable regime [Taylor vortex flo (TVF)].

The velocity variations are portrayed in Fig. 7 as functions of the spatial positions (i.e., z/d and r/r_e) for different Reynolds numbers and for the Newtonian fluid case ($n = 1$). The velocity modulus [Fig. 7(a)] shows that the flow goes inward and it develops mainly in the gap $0 \leqslant z/d \leqslant 0.8$ (and, symmetrically in the gap $3 \leqslant z \leqslant 3.8$). Although this flow develops rapidly when Re increases from 0 to 60, it seems to display an asymptotic value for a higher Re. In the central region of the annulus the flow is insignificant at low Reynolds numbers, and continues to increase for higher Reynolds numbers.

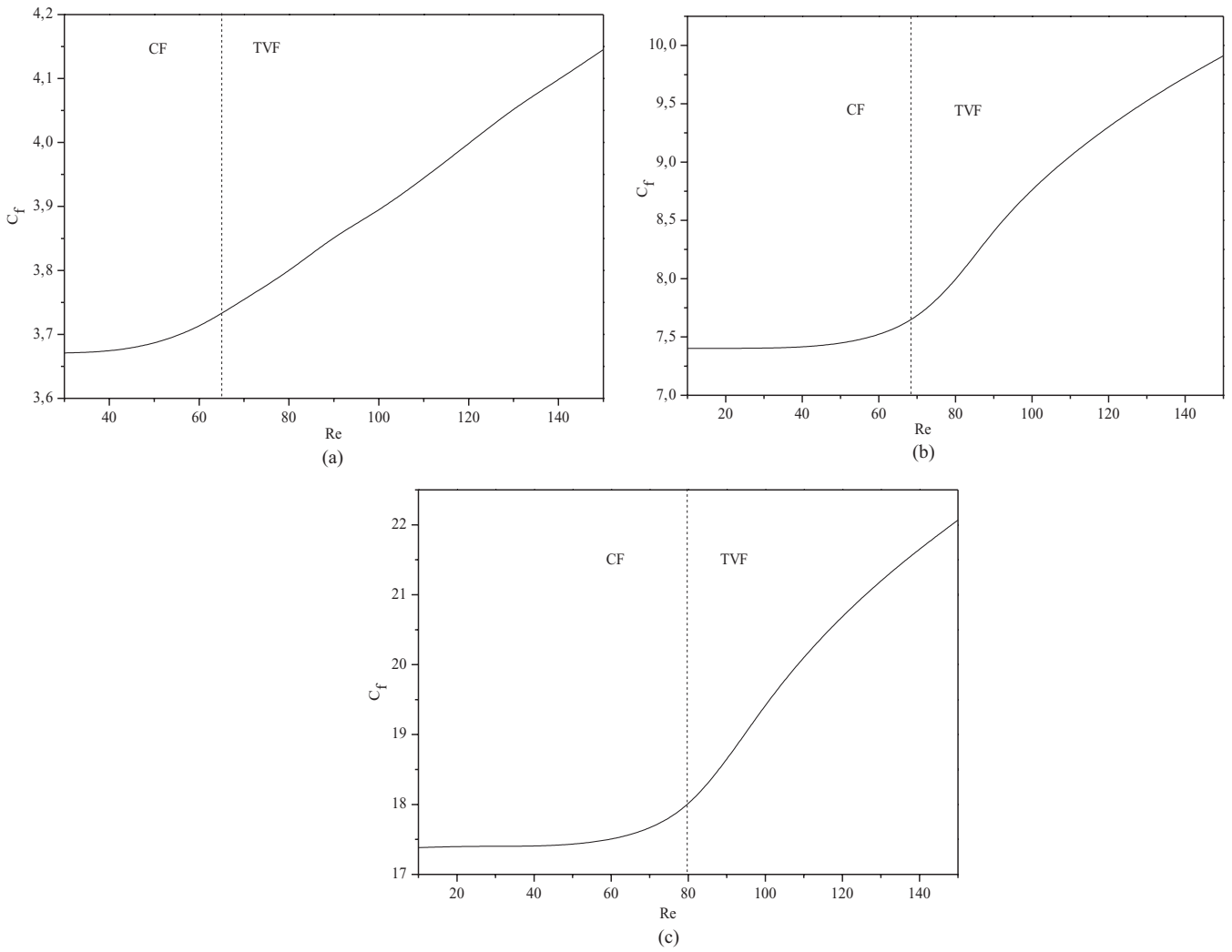

FIG. 11. Evolution of the friction factor versus Re for $\eta = 0.5$ and $\Gamma = 3.8$. (a) $n = 0.5$, (b) $n = 1$, and (c) $n = 1.5$.

Along the radial direction, the velocity [Fig. 7(b)] exhibits an extremum close to the midpoint of the gap. For Re = 40, this velocity component is almost zero. This suggests that, away from the end caps, the flow is of a type of Couette. For Re = 60, the radial velocity is negative in almost all the annular gap, but nevertheless remains low which coincides with the onset of the central cells. For the highest Reynolds numbers an inward flow is obtained in the cavity center according to the results of the streamlines.

The distribution of the axial velocity u_z and the radial velocity u_r in the median plan, portrayed in Figs. 7(c) and 7(d), confirms that the Ekman vortices are present at small rotation rates. At higher rotation rates, which, however, are still smaller than that corresponding to the critical Reynolds number, little cells appear between the Ekman cells. At supercritical rotation rate, these cells grow but remain, however, less intense than those of the extremities.

Figure 8 shows the evolution of the radial and axial velocities function of z/d for a Reynolds number of Re = 100. We notice that these velocity components vanish and change sign periodically along the channel, which means that the vortices rotate in opposite directions. In this figure, we note that the radial and the axial velocities grow when n decreases. This suggests that the flow intensity decreases with n according to the rheological behavior of the non-Newtonian fluids.

Figure 9 illustrates the combined effect of the Reynolds number and the power-law index on the stream function, azimuthal vortices contours, and azimuthal velocities. As for the Newtonian case, the flow chart begins with the formation of the Ekman cells close to the end walls. For the pseudoplastic fluid ($n = 0.5$), this structure is altered for Re = 50 where a weak cell begins to form in the neighborhood cavity walls. For dilatant fluids ($n = 1.5$) in Fig. 10, this transition occurs for, approximately, Re = 75. For a further increasing of the rotation rates, the Taylor cells become fully developed for Re = 65 in the case of the pseudoplastic fluid and for Re = 80 in the case of the dilatant fluid. Continuing to increase the value of the Reynolds number, we note that the flow structure changes again, from the four-cells to the two-cells regime at Re = 111.5 for the pseudoplastic fluid.

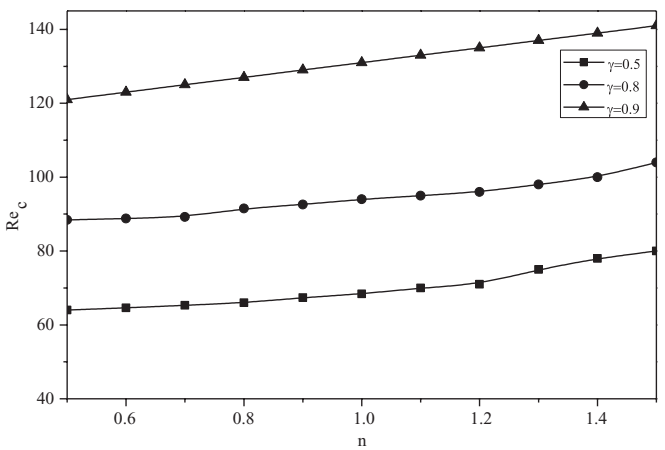

FIG. 12. Critical transition Reynolds number against n for different η.

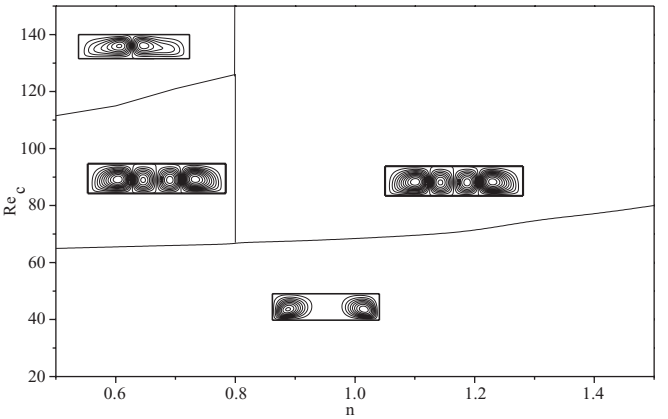

FIG. 13. Map of flow structures for power-law fluids for $\eta = 0.5$ and $\Gamma = 3.8$.

Figure 11 illustrates the evolution of the friction factor as a function of the Reynolds number for the short column ($\Gamma = 3.8$) with a large cross section ($\eta = 0.5$). For the Newtonian fluid [Fig. 11(b)] in the region Re $<$ Re$_c$, we note that C_f remains virtually constant for low Reynolds number values and it increases significantly when Re exceeds the value Re$_c$. For the pseudoplastic and dilatant fluids in Figs. 11(b) and 11(c), we note that in the TVF regime, the friction factor is more important. The vertical lines indicate the transition Reynolds number value from the Couette flow (CF) regime to the TVF regime. These positions were obtained by the visualization method, when the Taylor rolls occupy the whole annular space of the duct by increasing gradually the Reynolds number.

To resume the transition from the laminar stable regime (CF) to the laminar unstable regime (TVF) for different fluids, Fig. 12 shows the evolution of Re$_c$ versus the power-law index n for different radius aspect ratios. We can easily observe that Re$_c$ exhibits a monotonic increase with n. As the radius aspect ratio augments, the transition regime appears for higher critical Reynolds number.

Figure 13 presents a map of the flow structures for power-law non-Newtonian fluids for $\eta = 0.5$ and $\Gamma = 3.8$. According to the fact that the Reynolds number is limited in the range

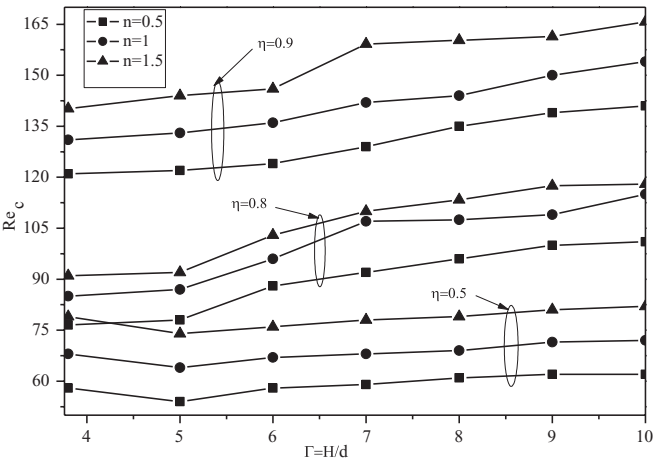

FIG. 14. Critical steady Reynolds number Re$_c$ versus aspect ratio Γ for the transition between two- and four-cell flows for $\eta = 0.5$.

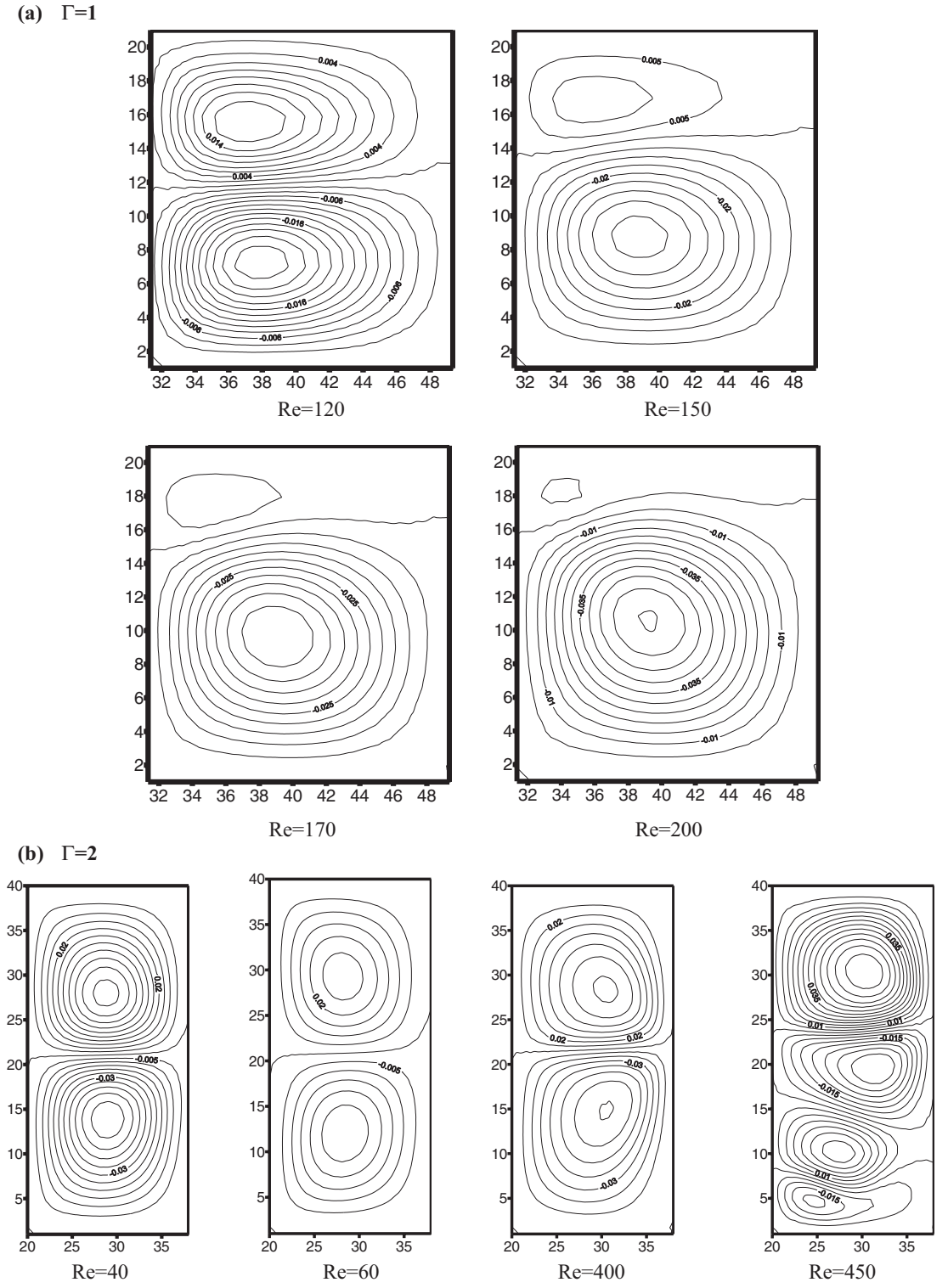

FIG. 15. (a), (b) Computed contours of the stream function lines of Newtonian fluid for different Γ at large radius ratio ($\eta = 0.5$).

20–150, the flow structure of pseudoplastic fluids exhibits a 2-4-2 cells regime while for the Newtonian and dilatant fluid the flow shows a 2-4 cells regime.

The influence of the aspect ratio and the radius ratio on the transition to the unstable laminar regime (TVF) in the short annular columns is shown in Fig. 14. It is observed that the critical Reynolds number increases with the increase of both aspect ratio and radius ratio for a given value of the shear-thinning index n. For a low radius ratio ($\eta = 0.5$) Re_c varies slightly with Γ, while for higher radius ratio the variation of Re_c is more important. For a reduced aspect ratio and the radius ratio ($\Gamma = 3.8$ and $\eta = 0.5$) the effects of the ends become gradually important which explains that Re_c is more important.

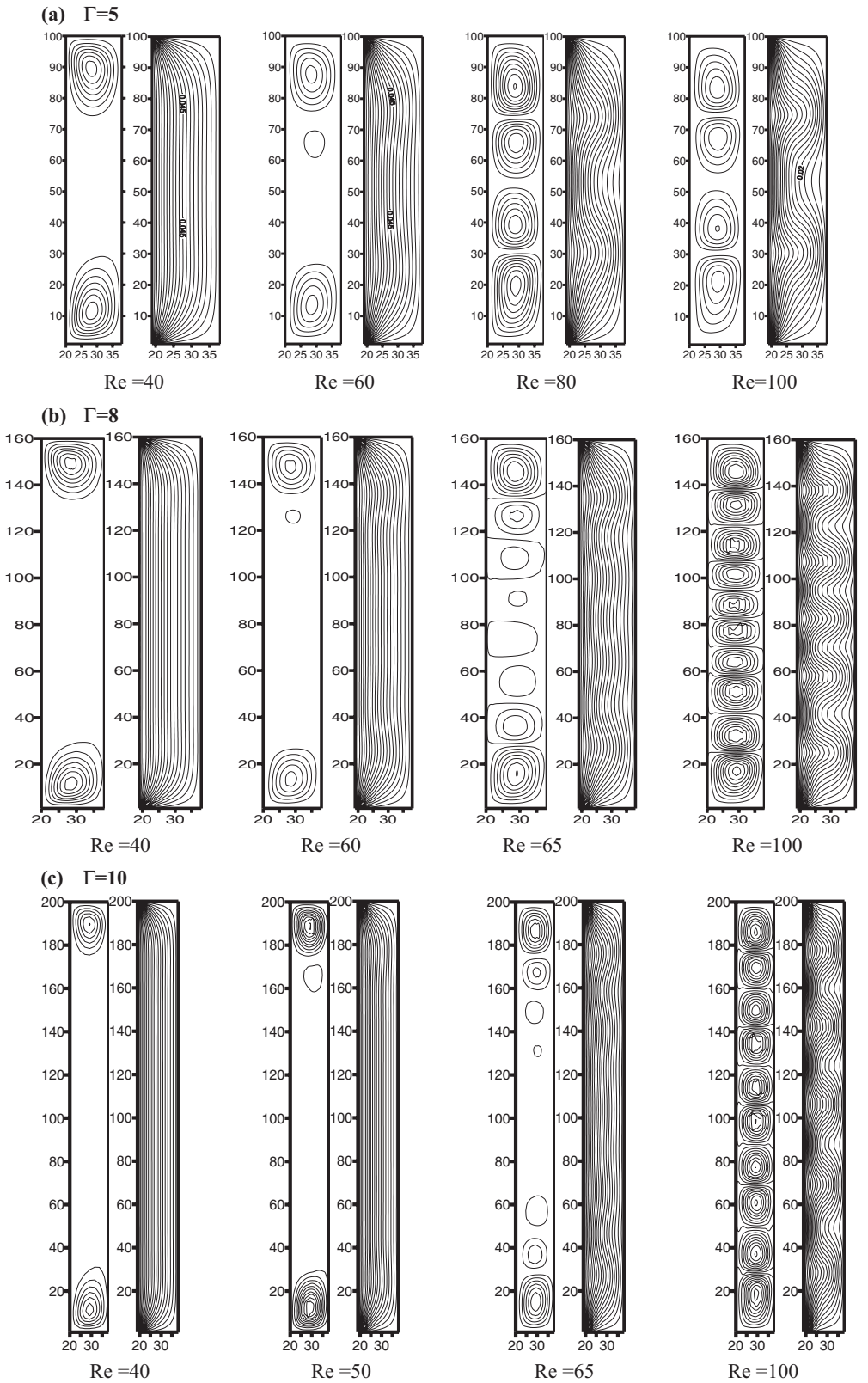

FIG. 16. (a)–(c) Computed contours of the stream function lines (left) and the azimuthal velocity (right) of Newtonian fluid for different Γ at large radius ratio ($\eta = 0.5$).

In Fig. 15(a), we note that for sufficiently small Reynolds numbers, the basic flow structure for the Newtonian case exhibits a symmetric two-cells state consisting of Ekman circulations induced by the end caps. The primary bifurcation from this two-cells state is to an asymmetric structure with a large cell and a small one in the corner close to the

inner cylinder. This choice of parameters leads to a smooth supercritical bifurcation to the one-cell mode as the Reynolds number is increased beyond a critical value. A lot of studies have been done in the very small aspect ratio case and Benjamin and Mullin [6] were the first to study this regime experimentally and confirm the existence of the one- and two-cell states. For an aspect ratio Γ of 2 in Fig. 15(b), the primary bifurcation coincides at the transition from the stable regime two-cell mode to the unstable regime four-cell mode. For larger aspect ratio, in Figs. 16(a)–16(c), for further increase in Reynolds number, we note the onset of a weak pair of cells in the center of the annuli. The centrifugal force effect in the annulus prevails on the viscous forces and the flow is dominated by the laminar unstable regime (TVF).

VI. SUMMARY

A numerical investigation is developed for a flow of non-Newtonian fluids between two concentric cylinders using the lattice Boltzmann method D2Q9 model. The inner cylinder rotates with a uniform velocity while the outer cylinder and end caps are kept at rest. Two kinds of aspect ratio are considered for the validation purpose, an infinite column and a finite column. For low Reynolds number, the present axisymmetric lattice Boltzmann code is validated against an analytical expression of velocity and available literature results for the Taylor-Couette flow at nonturbulent values of Re. The effect on the flow pattern of several parameters such as the Reynolds number and the power-law index are analyzed. The results show that when $\mathrm{Re} \geqslant \mathrm{Re}_c$, the flow changes from the stable laminar regime (CF) to the unstable laminar regime (TVF) and its structure switches from the two-cells to four-cells mode for both Newtonian and dilatant fluids. Contrariwise for pseudoplastic fluids, the flow exhibits 2-4-2 structure passes from two-cells to four-cells and switches again to the two-cells configuration. Furthermore, the critical Reynolds number presents a monotonic increase with n, and as the radius ratio grows, the transition flow regimes tend to appear for higher critical Reynolds number. In the short annular conducts, the basic flow is a symmetric two-cell state composed of an Ekman circulation induced by the ends.

[1] G. I. Taylor, Philos. Trans. R. Soc. London A **223**, 289 (1923).
[2] P. J. Blennerhassett, and P. Hall, Proc. Roy. Soc. London A **365**, 191 (1979).
[3] M. Lücke, M. Michelcic, and K. Wingerath, J. Fluid Mech. **140**, 343 (1984).
[4] T. B. Benjamin, Proc. R. Soc. London, Ser. A **359**, 1 (1978).
[5] T. B. Benjamin, Proc. R. Soc. London, Ser. A **359**, 27 (1978).
[6] J. A. Cole, J. Fluid Mech. **75**, 1 (1976).
[7] T. Mullin, G. Pfister, and A. Lorenzen, Phys. Fluids **25**, 1134 (1982).
[8] R. C. Diprima and P. M. Eagles, Phys. Fluids **27**, 2403 (1984).
[9] T. B. Benjamin and T. Mullin, Proc. R. Soc. London, Ser. A **337**, 221 (1981).
[10] K. Cliffe, J. Fluid. Mech **197**, 37 (1988).
[11] V. Sinevic, R. Kuboi, and A. W. Nienow, Chem. Eng. Sci. **41**, 2915 (1986).
[12] S. T. Wereley and R. M. Lueptow, J. Fluid Mech. **364**, 59 (1998).
[13] T. J. Lockett, S. M. Richardson, and W. J. Worraker, J. Non-Newtonian Fluid Mech. **43**, 165 (1992).
[14] M. P. Escudier, I. W. Gouldson, and D. M. Jones, Proc. R. Soc. London, Ser. A **449**, 155 (1995).
[15] M. Yoshino, Y. Hotta, T. Hirozane, and M. Endob, J. Non-Newtonian Fluid Mech. **147**, 69 (2007).
[16] D. Wang and J. Bernsdorf, Comput. Math. Appl. **58**, 1030 (2009).
[17] I. Halliday and L. A. Hammond, J. Phys. A **35**, L157 (2002).
[18] T. S. Lee, H. Huang, and C. Shu, Int. J. Mod. Phys. C **17**, 645 (2006).
[19] X. D. Niu, C. Y. Shu, and T. Chew, Int. J. Mod. Phys. **14**, 785 (2003).
[20] Y. Peng, C. Shu, Y. T. Chew, and J. Qiu, J. Comput. Phys. **186**, 295 (2003).
[21] H. Huang, T. S. Lee, and C. Shu, Int. J. Numer. Methods Fluids **53**, 1707 (2007).
[22] H. Huang, T. S. Lee, and C. Shu, Int. J. Num. Methods Heat Fluid Flow **17**, 587 (2007).
[23] H. Huang and X. Y. Lu, Phys. Rev. E **80**, 016701 (2009).
[24] H. Huang, Z. Li, S. Liu, X. Y. Lu, and S. Chen, Int. J. Numer. Methods Fluids **61**, 341 (2009).
[25] H. Huang, T. S. Lee, and C. Shu, Int. J. Numer. Methods Heat Fluid Flow **16**, 185 (2006).
[26] X. He and L. Luo, J. Stat. Phys. **88**, 927 (1997).
[27] T. S. Lee, H. Huang, and C. Shu, Int. J. Numer. Methods Fluids **49**, 99 (2005).
[28] J. G. Zhou, Phys. Rev. E **78**, 036701 (2008).
[29] J. G. Zhou, Phys. Rev. E **84**, 036704 (2011).
[30] A. Hongyan, Z. Chuhua, M. Jianping, and Z. Yonghao, Physica A **391**, 8 (2012).
[31] A. Brahim, C. Lemaitre, C. Nouar, and N. Ait-Moussa, J. Non-Newtonian Fluid Mech. **183-184**, 37 (2012).
[32] G. Cognet, Doctoral thesis, Université de Nancy, 1968.
[33] J. Peng and K. Q. Zhu, J. Fluid Mech. **512**, 21 (2004).
[34] Y. Liu, M.Eng. thesis, National University of Singapore, 1998.
[35] C. D. Andereck, S. S. Liu, and H. L. Swinney, J. Fluid Mech. **164**, 155 (1986).
[36] C. R. Di Prima and H. L. Swinney (Springer-Verlag, Berlin, 1981), pp. 139–180.
[37] Z. Guo, C. Zheng, and B. Shi, Phys. Fluids **14**, 2007 (2002).
[38] X. F. LI, G. H. Tang, T. Y. Gao, and W. Q. Tao, Int. J. Mod. Phys. C **21**, 1237 (2010).
[39] R. Nebbali and K. Bouhadef, Int. J. Therm. Sci. **50**, 1984 (2011).
[40] R. Nebbali and K. Bouhadef, Int. J. Numer. Methods Heat Fluid Flow **16**, 870 (2006).
[41] J. Peng and K. Q. Zhu, J. Fluid Mech. **512**, 21 (2004).

[42] D. Pirrô and M. Quadrio, Europe, J. Mech. B/Fluids **27**, 552 (2008).
[43] D. Coles, J. Fluid Mech. **21**, 385 (1965).
[44] P. Hall, Proc. R. Soc. London, Ser. A **372**, 317 (1980).
[45] L. Yang and B. Farouk, Int. J. Heat Mass Transfer **35**, 1947 (1992).
[46] V. Steinberg and A. Groisman, Philos. Mag. B **78**, 253 (1998).
[47] A. Groisman and V. Steinberg, Phys. Rev. Lett. **78**, 1460 (1997).
[48] R. G. Larson and E. S. G. Shaqfeh, S. J. Muller, J. Fluid. Mech. **218**, 573 (1990).